Applied Chemical Engineering (2026) Volume 9 Issue 2 ISSN: 2578-2010 (O)
doi: 10.59429/ace.v9i2.5986

RESEARCH ARTICLE

Synthesis, Anti-Cancer Activity, and Molecular Docking of New Co(II), Ni(II) and Cu(II)Complexes with an Imidazole-Azo Ligand

Ali Abdulhussein, Israa N.Witwit *

Department of Chemistry, Faculty of Science, University of Kufa, Najaf, Iraq

***Corresponding author:** Israa N.Witwit , israa.witwit@uokufa.edu.iq

ABSTRACT

Background: The development of metal-based therapeutics represents a significant advancement in medicinal inorganic chemistry. Here, the strategic synthesis and comprehensive characterization of a new imidazole-azo ligand, (E)-4-methyl-2-((4-phenoxyphenyl)diazinyl)imidazole (MPDI), are presented. Divalent transition metal complexes with Co(II), Ni(II), and Cu(II) were also investigated.

Methods: The compounds were characterized using 1HNMR, mass spectrometry, UV-Vis spectroscopy, and CHN analysis. Structural investigations, including molar conductivity and magnetic susceptibility measurements, confirmed a non-electrolytic octahedral geometry for all complexes. Scanning electron microscopy (SEM) revealed a significant morphological transformation from bulk microcrystalline ligands 5–20 μm to nano-sized, interconnected porous networks 100–250 nm in the Ni(II) complexes, attributed to the metal-template effect.

Results: Cytotoxicity was assessed against the MCF-7 breast cancer cell line using the MTT assay. Coordination resulted in a marked synergistic enhancement of bio-potency; the free ligand exhibited an IC50 of 1211.53 mu g/mL, while the Cu(II) complex demonstrated a 26.5-fold increase in efficacy with an IC50 of 45.70 \mu g/mL. Molecular docking simulations with the 5T92 protein (Estrogen Receptor Alpha) supported these results, revealing high binding affinities ranging from -15.26 to -17.24 kcal/mol. The Ni(II) complex showed the strongest theoretical affinity, stabilized by a unique π-cation interaction with ARG394.

Keywords: Azo-imidazole complexes; Nano-complexes; MCF-7 cytotoxicity; Molecular Docking; 5T92 Protein; Synergistic effect

ARTICLE INFO

Received: 20 April 2026
Accepted: 11 May 2026
Available online: 25 June 2026

1. Introduction

Azo-imidazole compounds are important ligands in coordination chemistry and other applied fields. Their sensitivity, visible color changes upon oxidation, and stability make them valuable [1-3]. These compounds exhibit biological activity and coordinate with various transition metals across multiple oxidation states [4]. Synergistic back-bonding with central metal ions occurs via vacant orbitals on the metal ions. The formation of a stable five-membered chelate ring between the metal and ligand further enhances complex stability. Appropriate substituents in azo-imidazole ligands promote interactions with amino acids, proteins, and DNA in cancer cell lines. They also enable permeation across bacterial cell membranes, thereby inhibiting biological functions [5-8]. This inhibition is stronger in coordination complexes with metal ions [9,10]. As a result, these compounds are promising candidates for evaluation as anticancer agents [11,12] and for treating pathogenic bacteria, particularly Gram-negative strains. Furthermore, cutting-edge strategies in metallodrug design have

demonstrated that copper complexes can integrate chemotherapy with catalytic in situ synthesis of therapeutic agents, paving the way for highly targeted dual-agent cancer therapies [13, 14]. In this work, we prepared and characterized a new azo-imidazole ligand based on 4-methylimidazole. We then examined its coordination to divalent cobalt, nickel, and copper ions. The anticancer activity of the free ligand and its copper complex was evaluated against breast cancer cells. A theoretical molecular docking study was also performed to investigate their binding affinity.

2. Experimental part

2.1. Chemicals and Apparatus

All chemicals utilized in this study were supplied by reputable companies, including Fluka, B.H.D., and AK Scientific, and possessed high purity. FT-IR measurements were performed with a Shimadzu 8400. Mass spectrometry was performed on a SCIEX-3200. Elemental analysis was carried out with a PerkinElmer 2400 Series II CHNS/O at the same institute. The electronic spectrum was measured with a Shimadzu UV-1650 spectrophotometer. Molar conductivity was determined using a 720-WTW at the University of Kufa, Faculty of Science, Iraq. The 1H NMR spectrum in DMSO-d6 was recorded on a Bruker DRX-500 spectrometer.

2.1.1. Preparation of (MPDI) ligand

The ligand (E)-4-methyl-2-((4-phenoxyphenyl)diazinyl) imidazole was synthesized via diazotization and coupling of 4-phenoxyaniline and 4-methylimidazole. The first step was to prepare a diazonium compound. 4-Phenoxyaniline (1.852 g, 0.01 mole) was dissolved in 25 mL of distilled water, and 3 mL of concentrated hydrochloric acid at below 5°C, and the mixture was treated drop-wise with sodium nitrite. This formed a diazonium salt by dissolving in about 10 mL of distilled water (0.7 g). To stabilize the diazonium intermediate, the solution was allowed to stand for 30 min. It was then released and dissolved in an ethanolic solution of 4-methylimidazole (0.82 g in 25 mL absolute ethanol). An orange precipitate formed after a few minutes, indicating successful formation of the azo compound. The product was washed with distilled water, dried, and recrystallized from hot ethanol. Scheme 1 shows the overall synthesis strategy.

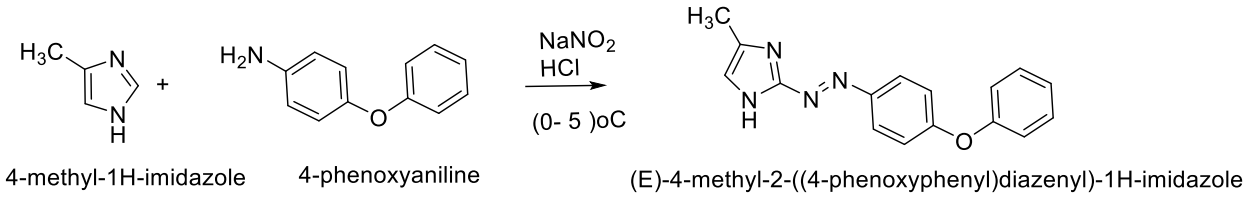

Scheme 1. General synthetic reaction for the ligand (MPDI).

2.1.2. Preparation of solid complexes

Solid complexes of divalent cobalt, nickel, and copper ions were synthesized at a molar ratio of 2:1 (metal: ligand) by slowly adding a ligand solution, prepared by dissolving 0.55 g of the compound in 20 mL of absolute ethanol, to the metal ion solution under continuous stirring. The formation of solid precipitates confirmed the completion of complexation; the precipitates were then separated, recrystallized from hot ethanol, and dried. Scheme 2 illustrates the overall reaction pathway in ordered solid complexes with the studied ligand.

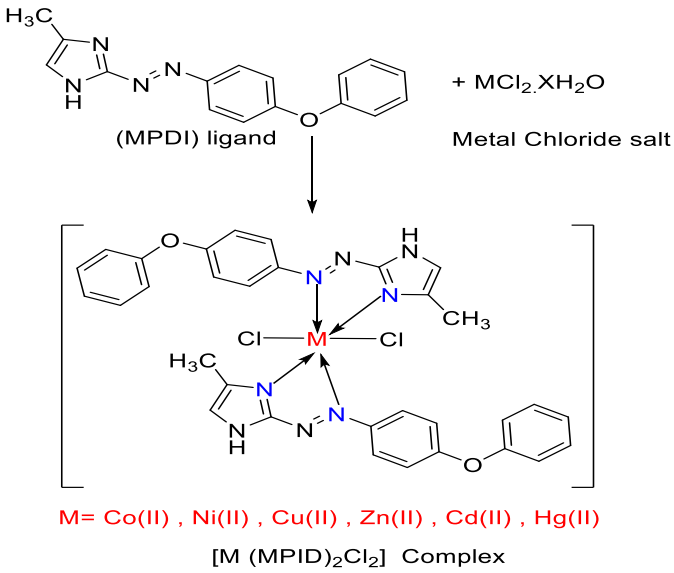

Scheme 2. The general synthetic reaction for the solid complexes.

2.2. Anti-cancer Activity

Cell lines and culture. MCF7 (human breast cancer cell line) and MCF10A (human breast normal cell line) were obtained from the National Cell Bank of Iran (Pasteur Institute, Iran). MCF7 Cells were cultured in RPMI-1640 medium (Gibco) with 10% FBS (Gibco), antibiotics (100 U/ml penicillin and 100 µg/ml streptomycin). Cells were cultured at 37 °C in humidified air supplemented with 5% CO_2 and subculture with trypsin/ethylene diamine tetraacetic acid (EDTA) (Gibco) in phosphate-buffered saline (PBS) solution.

MTT cell viability assay. Cell growth and cell viability were measured by the MTT [3-(4, 5-dimethylthiazol-2-yl)-2, 5-diphenyltetrazolium Bromide] (Sigma-Aldrich) assay. In short, dcells trypsinized, collected, diluted at a density of 1.4×10^4 cells/well and added to a 96-well plate containing 200 µl fresh media for each well before further expand on their monolayer, then treated with various concentrations (600-7.4 µg/ml) of the tested compounds in DMEM containing glucose for overnight incubation at 37 °C and 5% CO_2. At the end of treatment (24 h), the monolayer culture was left in the original plate undisturbed. Supernatant was discarded, and 200 µl/well of MTT solution (0.5 mg/ml in PBS) was added, and the plate was incubated for 4 h in the dark at 37 °C. Finally, after removing the MTT solution (supernatant from cells), dimethyl sulfoxide was added (100 µl per well). The solvent control (DMSO < 0.1%), the positive control, the number of independent replicates (n=3), and the specific statistical software used for the IC_{50} fitting procedure is Excel.

Cells were incubated in a shaker at 37 °C until crystals were fully dissolved. Absorbance was measured at 570 nm with an ELISA reader (Model Wave XS2, BioTek, USA) to quantify cell viability. IC50, the concentration of the compounds needed to achieve 50% of cell death, was determined from appropriate dose-response curves.

2.3. Molecular docking

All the docking and scoring calculations were performed using the molecular operation environment software (MOE) (Molecular Operating Environment (MOE), 2019). The crystal structure of the (ESTROGEN RECEPTOR ALPHA LIGAND BINDING DOMAIN IN COMPLEX WITH (2E)-3-{4-[(1R)-2-(4-fluorophenyl)-6-hydroxy-1-methy l-1,2,3,4- tetrahydroisoquinolin-1-yl]phenyl}prop-2-enoic acid) (PDB ID: 5T92) at a resolution of 2.22 Å was obtained from the Protein Data Bank. A resolution between 1.5 and 2.5 Å is considered a good quality for docking studies. It is known that the best score of RMSD values should be near 2 Å with an energy score less than or equal to -7 kcal/mol. These two values are often used as criteria to validate the result of the molecular docking.

3. Results and discussion

3.1. ^{1}H-NMR of (MPDI) ligand

The free ligand was analyzed using ^{1}H-NMR spectroscopy in DMSO-d^{6}, which helped determine its chemical structure. The spectrum showed a singlet at 12.94 ppm, corresponding to the (NH) proton of the imidazole ring (s, 1H, NH imidazole) [15]. A peak at 8.21 ppm was assigned to the protons of the phenyl ring located ortho to the (N=N) group (d, J = 8.5 Hz, 2H, Ar-H ortho to N=N). The CH protons of the imidazole and the terminal Ar-H rings appeared as multiple signals between 7.50 and 7.97 ppm (m, 6H, Ar-H terminal ring + Imidazole CH). Peaks at 7.17 ppm were attributed to the protons of the phenyl ring in the ortho position relative to the O-ether group (d, J=8.5 Hz, 2H, Ar-H ortho to O-ether). Finally, a singlet for the methyl protons appeared at 2.27 ppm (s, 3H, CH_3), as shown in the figure 1.

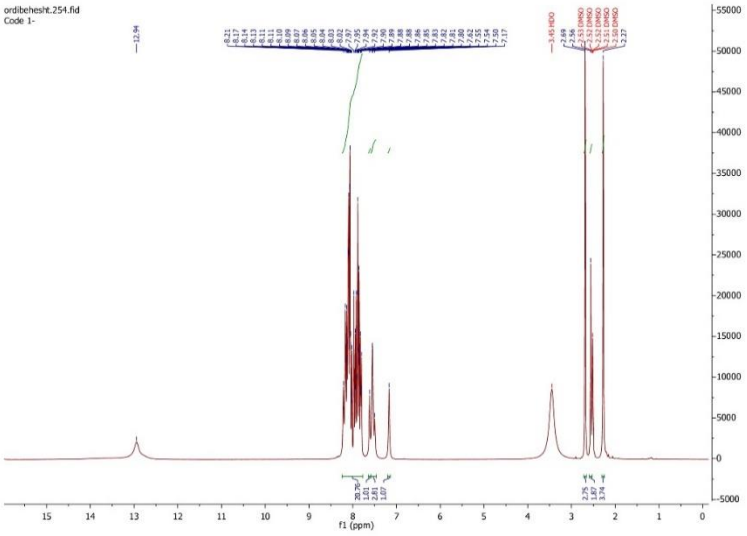

Figure 1. ^{1}HNMR spectrum of (MPDI) ligand.

3.2. Mass spectra of the (MPDI) ligand

Mass spectrometry plays a critical role in elucidating the molecular structure of the ligand and its fragmentation pathways. The mass spectrum of the free ligand (MPDI), as presented in Figure 2 and Scheme 3, reveals the molecular ion $[C_{16}H_{14}N_4O]^+$ at m/z 278.3, confirming the ligand's structure. The proposed fragmentation mechanism consists of two principal pathways, both initiated by cleavage of the azo group, resulting in the release of nitrogen gas (N_2). This initial step is well documented in previous qualitative studies on azo compound fragmentation. The process yields the ion fragment $[C_6H_{14}N_2O]^+$ at m/z 250.3, which exhibits a relative abundance of 100%.

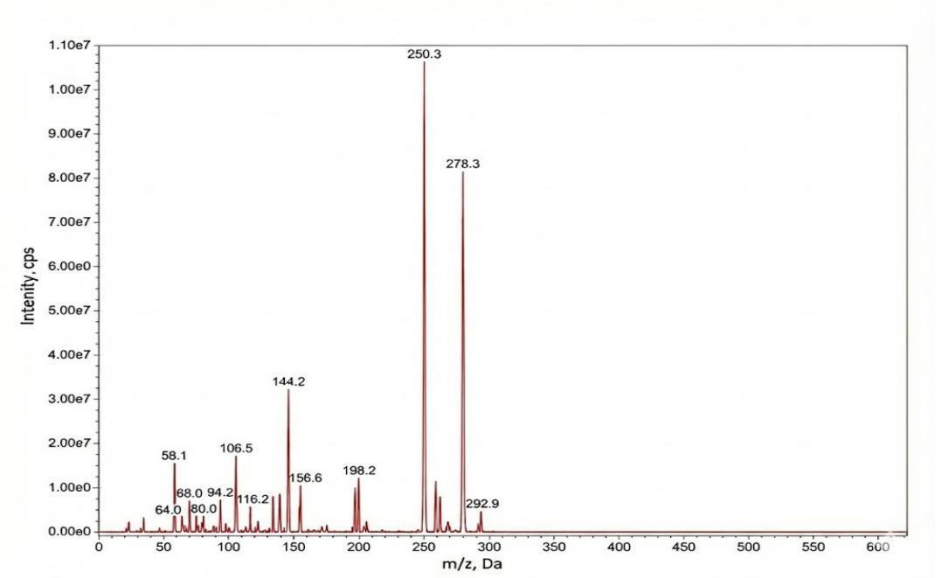

Figure 2. Mass spectrum of (MPDI) ligand.

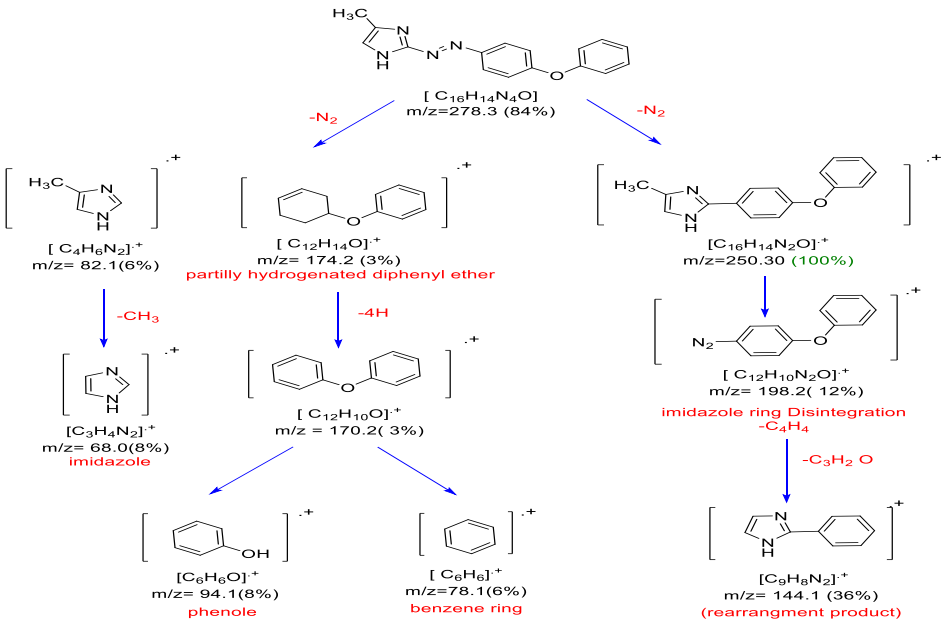

Scheme 3. General pathways for the fragmentation of the ligand (MPDI).

3.3. SEM analysis

Scanning electron microscopy reveals that complexation alters the Ni(II) ion as an example material's shape. The uncomplexed MPDI ligand forms nonporous, irregular macrocrystals between 5 and 20 micrometers in size. This compact structure points to strong π-π* stacking and self-assembly without a metal center, While comparing with one of its complexes with the Ni (II) ion. When Ni (II) is added, much smaller particles form, measuring 100-250 nanometers.

The [Ni (MPDI) $_2$ Cl_2] complex forms a connected, spongy, porous network composed of spherical and nearly spherical nanoparticles. The smaller size arises from the Metal-Template Effect, in which the Ni (II) ion directs the arrangement of azo-imidazole groups. During complexation, nucleation occurs faster than crystal growth, a common phenomenon in coordination polymer synthesis. This rapid nucleation prevents random clumping and yields particles in a narrow size range, unlike the broader distribution seen with free ligand. The spongy structure is important for chemistry, Large MPDI units and chloride ligands add bulk, and preventing particles from packing tightly and leaving empty spaces that create porosity. The spherical shape

lowers surface energy. Because the nano complex has a high surface-to-volume ratio, more active sites are exposed, as shown in figures 3-6.

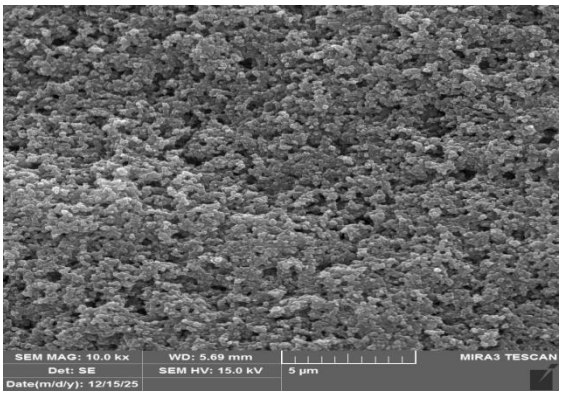

Figure 3. SEM of $[Ni(MPDI)_2Cl_2]$ at 5 µm.

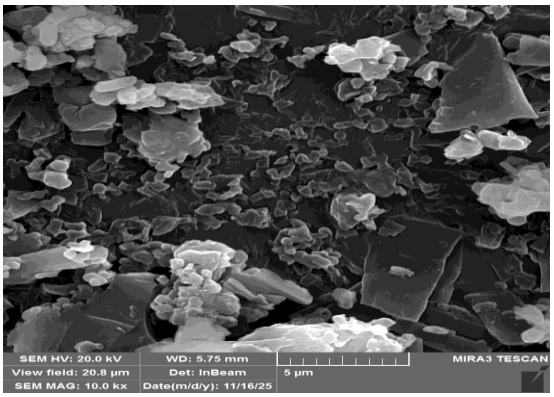

Figure 4. SEM of (MPDI)ligand at 5 µm.

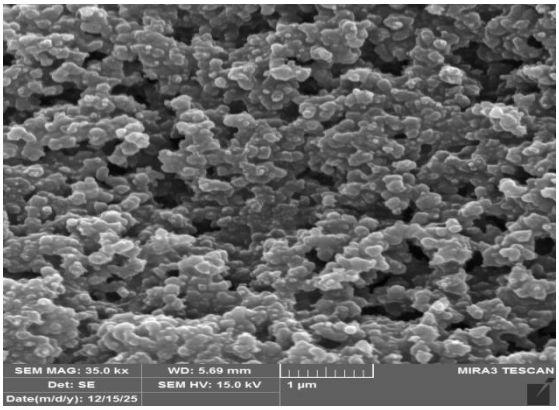

Figure 5. SEM of $[Ni(MPDI)_2Cl_2]$ at 1 µm.

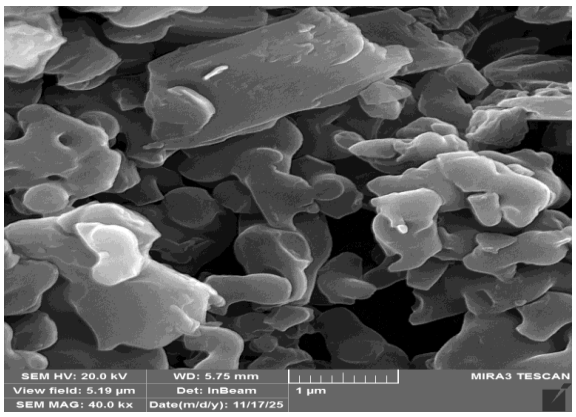

Figure 6. SEM of (MPDI) ligand at 1 µm.

3.4. Electronic Transitions

The electronic transitions of the ligand and its complexes were studied in the 200–900 nm range. Two bands at 205 and 245 nm are attributed to π–π* transitions in distinct aromatic ring environments, while a third band at 393 nm is ascribed to intra-ligand charge transfer and shows a clear red shift in the complexes. This shift, explained by metal-to-ligand charge transfer (MLCT) upon coordination, is illustrated in the figures and tables. The observed trend (Co < Ni < Cu) indicates that electronic transition energy depends on the metal ion[16] Therefore, the magnitude of the red shift directly reflects the strong regulatory effect of the specific metal ion on the electronic structure of the ligand. , reflecting each complex's electron configuration and d-orbital properties. Coordination stabilizes the ligand's π* orbitals and lowers the energy gap. The small shift in the Co (II) complex arises from its d^7 configuration, which requires more energy for electron transfer. The Ni (II) complex, with a d^8 configuration, shows a larger shift because it donates electrons more readily, while the Cu(II) complex, with a d^9 configuration, displays the largest shift. The high electron count and octahedral geometry of Cu (II) complexes facilitate electron transfer from the metal to the ligand. Additionally, Jahn-Teller distortion in octahedral Cu(II) complexes removes orbital degeneracy, creating a low-energy pathway for electron transfer to the ligand's π* system and minimizing the HOMO-LUMO gap [17], as shown in figures 7-10 and table 1.

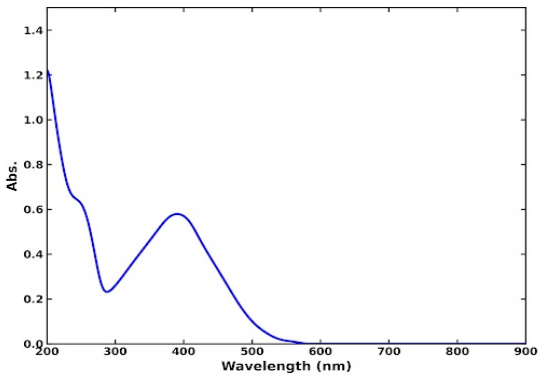

Figure 7. UV-Vis of (MPDI) ligand.

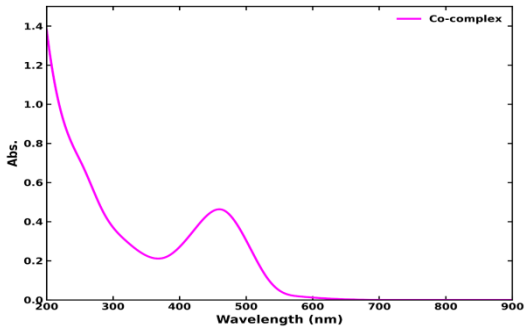

Figure 8. UV-Vis of $[Co(MPDI)_2Cl_2]$.

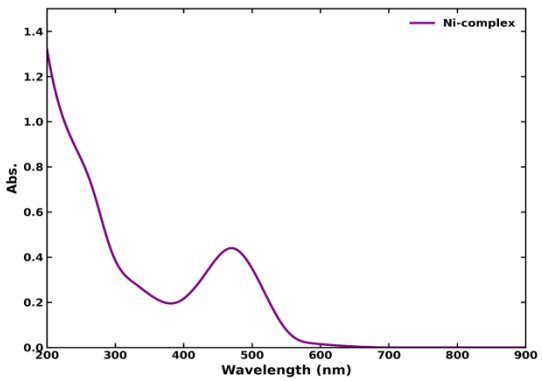

Figure 9. UV-Vis of $[Ni\ (MPDI)_2Cl_2]$.

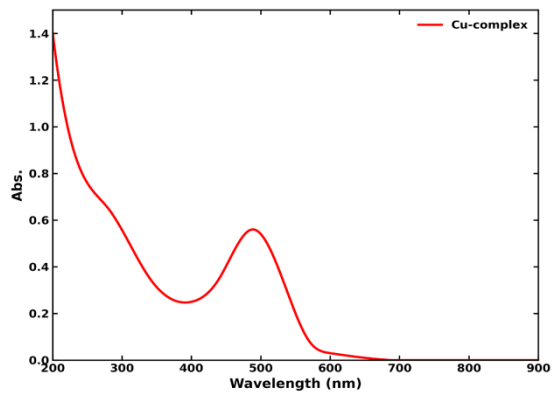

Figure 10. UV-Vis of $[Cu\ (MPDI)_2Cl_2]$.

Table 1. Types of electronic transitions of the (MPDI), and its complexes at (10^{-4}) M using ethanol solvent.

Compound	Electronic Transitions (nm)	Assignment
(MPDI)	205	π- π* (Aromatic)
	245	π- π* (Resonance)
	393 (ε=7×10^3 L .mol-.cm-)	n- π* (ILCT)
$[Co(MPDI)_2Cl_2]$	225	π- π* (Aromatic)
	255	π- π* (Resonance)
	465 (ε=4.6×10^3 L .mol-.cm-)	CT (MLCT)
$[Ni(MPDI)_2Cl_2]$	228	π- π* (Aromatic)
	265	π- π* (Resonance)
	471(ε=4.4×10^3 L .mol-.cm-)	CT (MLCT)
$[Cu(MPDI)_2Cl_2]$	230	π- π* (Aromatic)
	280	π- π* (Resonance)
	488 (ε=4.4×10^3 L .mol-.cm-)	CT (MLCT)

3.5. Magnetic susceptibility, Molar Conductivity, and Element Analysis

Magnetic moment (μeff) measurements for the synthesized complexes were conducted at room temperature (298 K) to determine the coordination geometry and electronic configuration of each central ion. The results indicate significant orbital involvement in addition to spin contribution, as evidenced by the experimental μeff value of 4.90 B.M, which exceeds the spin-only value for [Ar] $3d^7$ in an octahedral environment [18,19]. The Ni(II) complex exhibits a μeff of 3.12 B.M, which falls within the range of 2.80–3.50 B.M, confirming a high-spin d8 octahedral system [20]. The Cu (II) complex displays a μeff value of 2.30 B.M,

which is higher than the spin-only value (μeff s.o = 1.73 B.M), supporting the presence of orbital contribution. This increase is attributed to Jahn-Teller distortion affecting the system's spin-orbit coupling [21-23], Elemental microanalysis showed strong agreement between calculated and experimental values, confirming the molecular formulas of the synthesized compounds. Compared to theoretical predictions, molar conductivity measurements in methanol and DMSO also revealed non-electrolytic behavior, indicating the absence of external counter-ions. The silver nitrate test further supported this conclusion: adding $AgNO_3$ to the complex samples did not produce silver chloride (AgCl) precipitation [24,25], providing clear evidence that the chloride ions are coordinated within the inner coordination sphere, as shown in Table 3

Table 2. Some physical properties, molar conductivity values, element analysis of the ligand, and its complexes.

Compound	Color	m.p	Molar conductivity		Element Analysis Calc. (Found)		
			Methanol	DMSO	C	H	N
(MPDI)	Orange	146-148	----	-----	69.05 (69.23)	5.07 (5.08)	20.13 (20.25)
$[Co(MPDI)_2Cl_2]$	Brown	226-228	27.6	23.3	55.99 (56.00)	4.11 (4.12)	16.32 (16.34)
$[Ni(MPDI)_2Cl_2]$	Brown	231-233	27.2	23.0	56.01 (56.05)	4.11 (4.13)	16.33 (16.38)
$[Cu(MPDI)_2Cl_2]$	Dark Brown	254-256	25.8	20.6	55.62 (55.70)	4.08 (4.10)	16.21 (16.23)

3.6. Coordination Suggested Structure

Analytical data indicate that all synthesized complexes possess an octahedral geometry. The ligand forms a five-membered chelate ring by simultaneously coordinating to the central metal ion through the nitrogen atom of the azo bridge and the N3 nitrogen of the imidazole ring. The remaining coordination sites within the coordination sphere are occupied by two chloride ions, which preferentially adopt Trans positions, as illustrated in Figure 11.

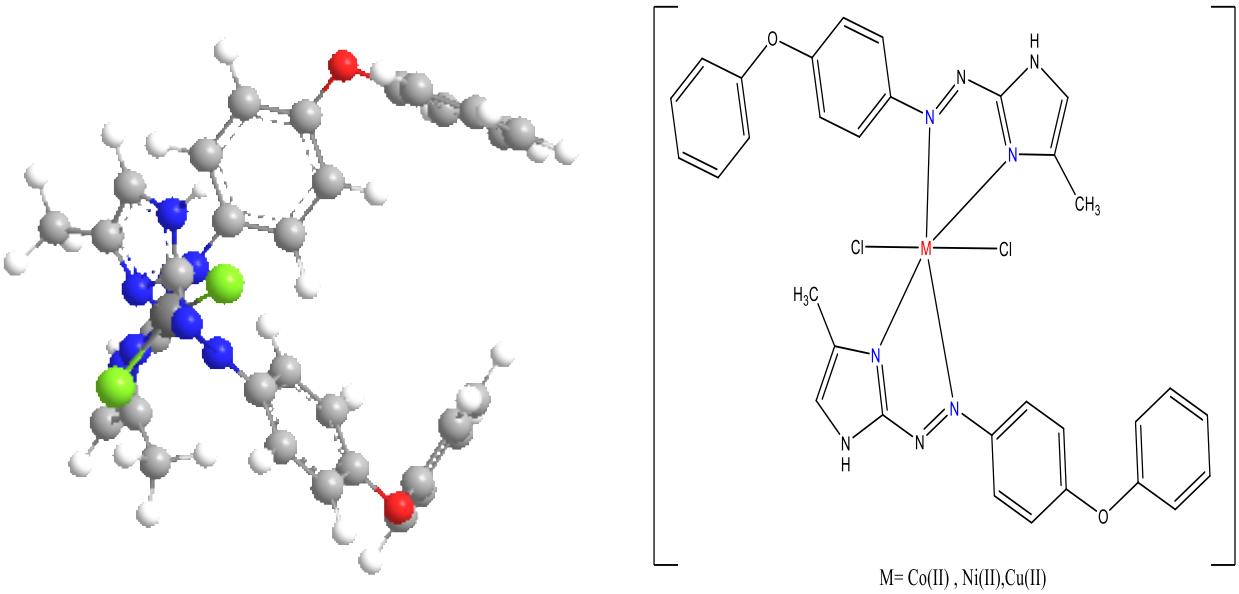

Figure 11. Suggested 2D, and 3D $[M(MPDI)_2Cl_2]$ complex structure.

3.7. Anti- Cancer Activity

The in vitro cytotoxicity of the azo-imidazole ligand (HMPDI) and its copper (II) complex [Cu $(MPDI)_2$ Cl_2] was evaluated against MCF-7 breast cancer cells. The IC_{50} results indicate a substantial increase in potency after coordination. The free ligand exhibited a high IC50 value (1211.53 µg/mL), indicating limited inhibition of cancer cell proliferation. In contrast, [Cu $(MPDI)_2Cl_2$] displayed significantly greater cytotoxicity due to physiological redox capabilities, with an IC_{50} of 45.70 µg/mL, representing an approximately 26.5-fold increase in efficacy. These findings indicate that the enhanced anticancer effect arises from a synergistic interaction between the ligand and copper, rather than merely the additive effects of the individual components. Tweedy's Chelation Theory largely explains the complex's increased activity. In the free ligand, polar groups such as imidazole and azo nitrogen atoms have difficulty penetrating the lipid-rich cell membrane. When chelated to the Cu (II) ion, the metal shares its positive charge with HMPDI donor atoms, increasing pi-electron delocalization in the chelate ring.

This redistribution of electron density substantially reduces the polarity of the metal center and increases the complex's lipophilicity. As a result, the complex can traverse the semipermeable cell membrane more efficiently than the free ligand, enabling greater uptake and retention within the intracellular environment.

The proposed octahedral geometry is central to the mechanism of action. The incorporation of two bidentate azo-imidazole ligands and two chloride ions results in a configuration that is both stable and reactive. Copper exhibits a well-documented capacity for redox cycling between the Cu (II) and Cu (I) oxidation states within the reductive intracellular environment of cancer cells. While the exact mechanism of cell death was not explicitly investigated in this study using flow cytometry or ROS-scavenging assays, literature on related Cu(II) azo-imidazole complexes suggests that the enhanced cytotoxicity may hypothetically proceed via a ROS-mediated apoptotic pathway. Future mechanistic studies will focus on confirming this proposed pathway. As a result, the oxidative stress induces mitochondrial dysfunction and irreversible DNA damage in MCF-7 cells, ultimately activating the apoptotic pathway. Furthermore, the octahedral arrangement is likely to optimize the orbital overlap necessary for these electron-transfer processes.

In comparison to reported literature values for Cisplatin, the clinical benchmark for chemotherapy with a typical IC_{50}f (5-25) mu g/mL in MCF-7 cells [21], the prepared copper (II) complex demonstrates a promising pharmacological profile. While Cisplatin exhibits a lower absolute IC_{50} value, copper-based complexes are widely discussed in the literature for their potential advantages in biocompatibility, as copper is an essential trace element with well-defined metabolic pathways in human cells. Structurally, these properties suggest a potentially favorable selectivity index and reduced systemic side effects compared to platinum-based therapies; nevertheless, comprehensive comparative trials are necessary to fully validate these biosafety assumption.

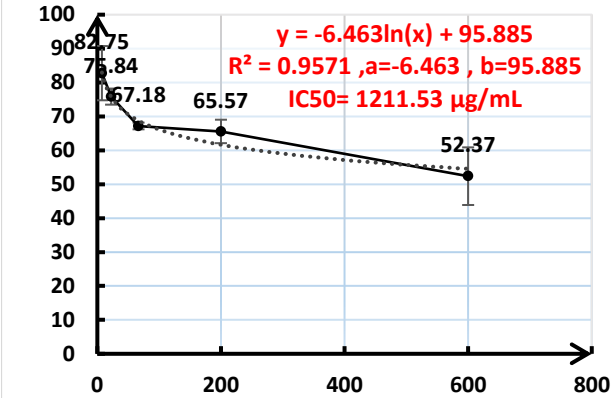

Figure 12. Dose-response curve of (MPDI) ligand for the MCF-7 breast cancer cell viability with different concentrations.

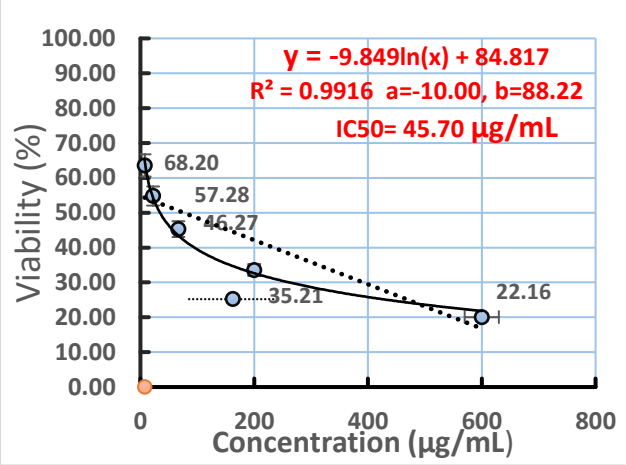

Figure 13. Dose-response curve of Cu(II) complex for the MCF-7 breast cancer cell viability with different concentrations.

Figure 14. Cytotoxic effect of. [Cu $(MPDI)_2Cl_2$] at 200 (µg/mL) towards MCF10 A cell lines.

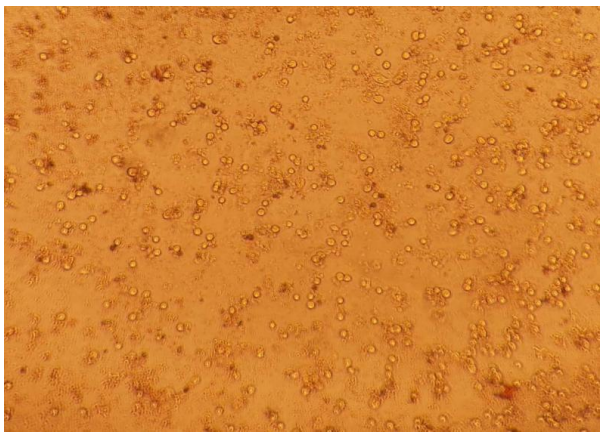

Figure 15. Cytotoxic effect of. (MPDI) at 200 (µg/mL) towards MCF10 A breast cancer cell lines.

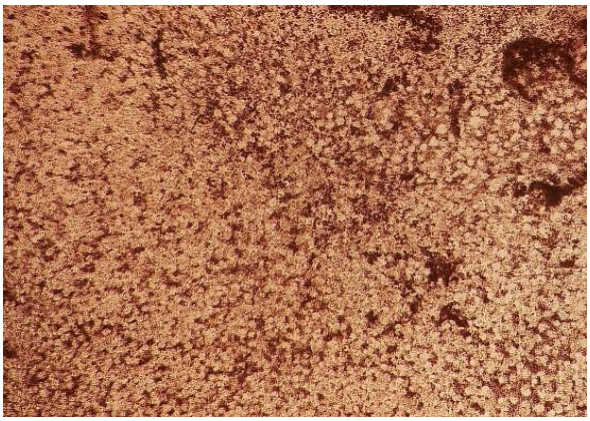

Figure 16. Cytotoxic effect of. [Cu $(MPDI)_2Cl_2$] at 200 (µg/mL) towards MCF-7 breast cancer cell lines.

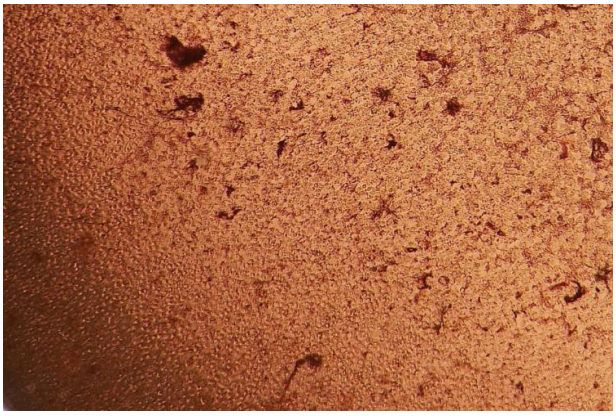

Figure 17. Cytotoxic effect of. (MPDI) at 200 (µg/mL) towards MCF-7 breast cancer cell lines.

Table 3. Dose -Response Data of Free ligand towards MCF-7 breast cancer cell lines.

Concentration (µg/mL)	7.4		22.22		66.66		200		600	
absorption at 570 nm	0.552	0.633	0.531	0.555	0.476	0.486	0.452	0.487	0.332	0.418
Viability (%)	77.09	88.41	74.16	77.51	66.48	67.88	63.13	68.02	46.37	58.38
Average Viability (%)	82.75		75.84		67.18		65.57		52.37	
Standard Deviation (±)	8.00		2.37		0.99		3.46		8.49	

Table 4. Dose -Response Data of Cu(II) complex towards MCF-7 breast cancer cell lines.

Concentration (µg/mL)	7.4		22.22		66.66		200		600	
absorption at 570 nm	0.455	0.521	0.392	0.428	0.342	0.338	0.240	0.487	0.144	0.203
Viability (%)	63.57	72.82	54.79	59.77	45.29	47.24	33.57	36.85	20.07	24.24
Average Viability (%)	68.20		57.28		46.27		35.21		22.16	
Standard Deviation (±)	6.54		3.52		1.38		2.32		2.95	

3.8. Molecular Docking study

The docking analysis of the free ligand and its complexes against the 5T92 protein demonstrates a distinct binding profile The Free ligand, in its optimal pose, presents a binding affinity of approximately −7.92 kcal/mol and an RMSD of 2.04 Å, serving as a robust reference for comparison. In contrast, Cu(II), Co(II), and Ni(II) complexes significantly stronger binding affinities of −15.26, −15.29, and −17.24 kcal/mol, respectively, each with RMSD values within the acceptable range of 1.08 to 1.79 Å. These findings indicate that these three complexses have much greater theoretical affinity for the 5T92 active site than the standard, and their predicted poses are both stable and well-defined. Notably, Ni(II) complex achieves the most negative docking score and maintains a stable RMSD of 1.78 Å, indicating the best fit ,Co(II) complex closely matches Cu(II) complex in binding energy, but the slightly lower RMSD of compound Cu(II) complex suggests that forms a more compact geometric orientation within the binding site, while compound Co(II) complex is still highly favorable and structurally plausible. Detailed analysis of interaction profiles clarifies the molecular basis for the observed binding strengths: Cu(II) complex is stabilized by hydrogen-bond donor interactions with MET343 and an acceptor contact with a structural water molecule, along with several π–H interactions with THR347 and LEU525, offering a combination of directional binding and surface complementarity. Co(II) complex forms strong hydrogen-bond donor interactions with THR347 and extensive π–H interactions with LEU387, PHE404, PHE425, and MET421, reflecting broader engagement with the aromatic region of the active site and benefiting from dispersion-type stabilization. Ni(II) complex, being the strongest binder, exhibits the most extensive pattern, including hydrogen-bond donor contacts with MET421 and ASP351 as well as a π-cation interaction with ARG394. The presence of the π-cation interaction, where the ligand's aromatic system is positioned near a positively charged side chain, is particularly significant for stabilization. This combination of multiple hydrogen bonds and a charged aromatic interaction likely explains why Ni(II) complex outperforms all other ligands and the standard in docking energy. Although the Ni(II) complex exhibited the highest theoretical binding affinity in silico, the Cu(II) complex was prioritized for the in vitro biological evaluation

due to copper's well-established physiological redox cycling capacity (Cu^{2+}/Cu^{1+}), which is highly relevant for inducing intracellular oxidative stress and cytotoxicity.

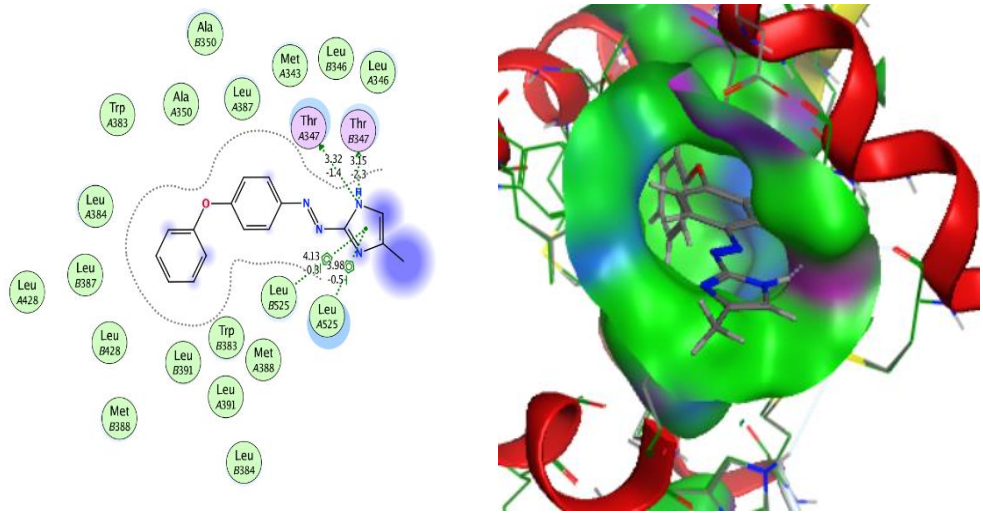

Figure 18. 2D and 3D interaction between (PDB ID: 5T92) protein and free ligand.

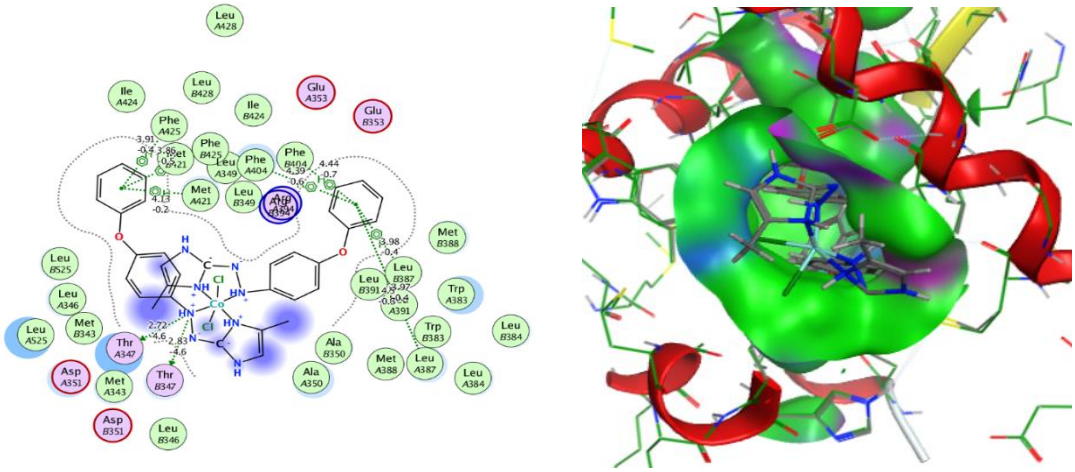

Figure 19. 2D and 3D interaction between (PDB ID: **5T92**) protein and $[Co(MPDI)_2Cl_2$.

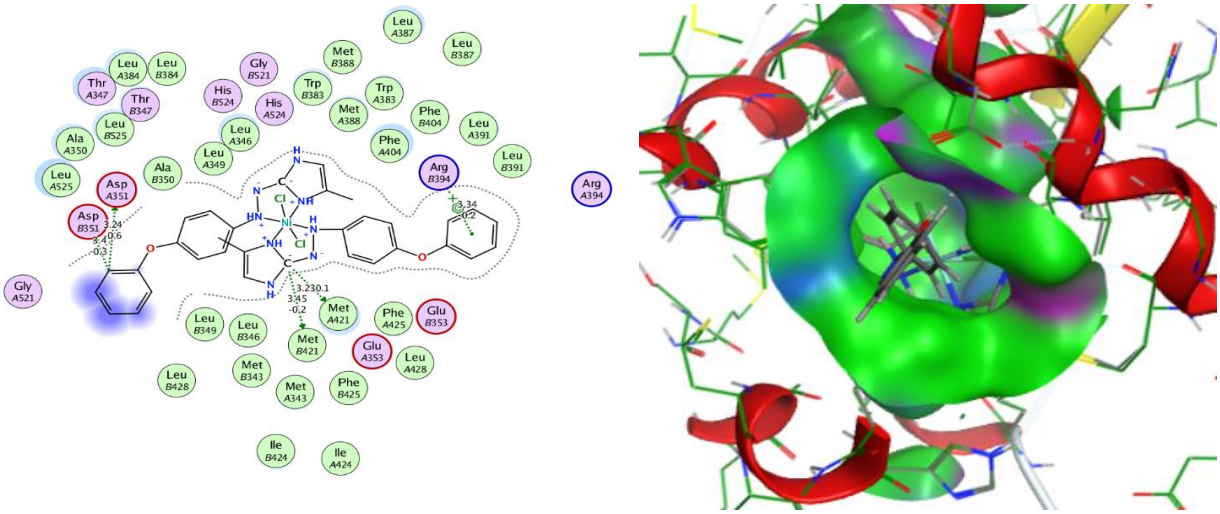

Figure 20. 2D and 3D interaction between (PDB ID: **5T92**) protein and $[Ni(MPDI)_2Cl_2]$.

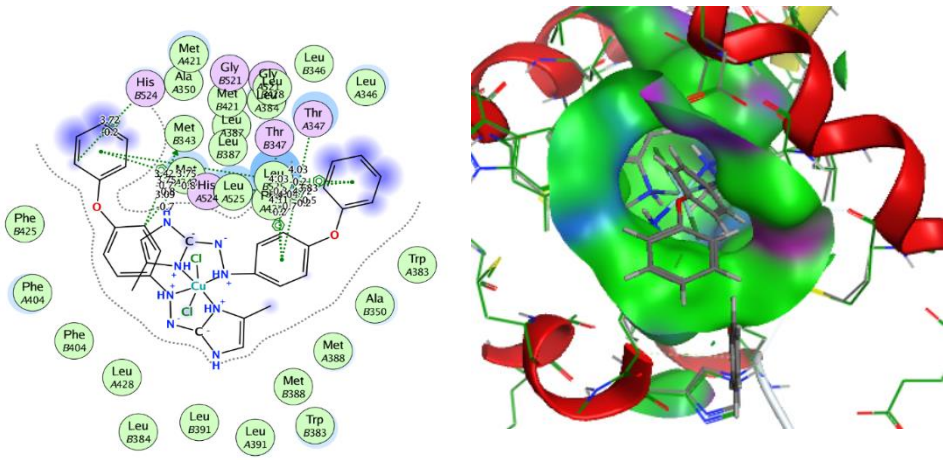

Figure 21. 2D and 3D interaction between (PDB ID: **5T92**) protein and $[Cu(MPDI)_2Cl_2]$.

4. Conclusions

The findings directly support Tweedy's chelation theory. Enhanced lipophilicity and reactive pathways was identified as key drivers of the observed anticancer activity. This study establishes a robust framework for the development of azo-imidazole metallopharmaceuticals as potent, biocompatible alternatives to conventional platinum-based therapies.

References

1. Mahdy, A.R.E., Abu Ali, O.A., Serag, W.M., Fayad, E., Elshaarawy, R.F.M. and Gad, E.M. (2022) 'Synthesis, characterization, and biological activity of Co(II) and Zn(II) complexes of imidazole-based azo-functionalized Schiff bases', Journal of Molecular Structure, 1259, 132726.
2. Balsa, L.M., Baran, E.J. and León, I.E. (2023). Copper complexes as antitumor agents: In vitro and in vivo evidence, Current Medicinal Chemistry, 30(5): 510–557.
3. Mohammed, A. Q.; Al-Jeboori, A. J. (2020), Synthesis and Characterization of Mixed Ligand Complexes of Azo-Imidazole and 2,2′-Bipyridine with Some Transition Metals. Journal of Physics: Conference Series, 1664(1).
4. Misra, T. K.; Sinha, C. Synthesis, Characterization and Redox Studies of Iron(II) and Iron(III) Complexes with 1-Methyl-2-(Arylazo) imidazoles (1999). Transition Metal Chemistry, 24 (2):172–177.
5. Hossain, M. S.; Jesmin, M. 2012, Synthesis, Characterization and Antimicrobial Activity of Transition Metal Complexes with Azo-Imidazole Derivatives. Journal of the Serbian Chemical Society 77 (10), 1401–1413.

6. Gaber, M.; El-Ghamry, H. R.; Fathalla, S. K.(2022). Synthesis, Characterization, and Biological Evaluation of New Transition Metal Complexes Based on a Novel Azo-Imidazole Ligand as Potential Anticancer and Antimicrobial Agents. Sci. Rep. 12(20115).
7. Hassan, A. S.; Moustafa, G. O.; Morsy, N. M.(2023). New Azo-Imidazole Transition Metal Complexes: Synthesis, Characterization, DNA Binding, and In Vitro Anticancer Activity. Journal of Molecular Stracture. 1275(1).
8. Al-Noor, T. H.; El-Ajaily, M. M.; Maihub, A. A.(2022) Preparation, Characterization and Biological Activity of Some Metal Complexes with New Azo-Imidazole Ligand and 1,10-Phenanthroline. Journal of Physics .: Conference Series. 2022, 2322.
9. Al-Adilee, K. J.; Abass, A. K.; Taher, M. A.(2007) Synthesis, Characterization, and Biological Activity of Some Transition Metal Complexes of a New Azo-Imidazole Ligand. Molecules, 12 (5).
10. Mahmoud, W. H.; Deghadi, R. G.; Mohamed, G. G. (2021),Synthesis, Characterization and Biological Activity of Some Transition Metal Complexes of New Azo-Imidazole Ligand. Applied Organometallic Chemistry, 35 (2).
11. Zhu, M., Xu, S., Li, G., Xu, G., Zhang, Z., Liang, H., & Yang, F. (2025). Development of a high efficacy and low toxicity cobalt(II) agent for targeting inhibition of tumor growth through mitochondrial damage-mediated chemotherapy and immunotherapy. *Journal of Medicinal Chemistry*, 68, 13113–13126.
12. Jiang, M., Li, W., Liang, J., Pang, M., Li, S., Xu, G., Zhu, M., Liang, H., Zhang, Z., & Yang, F. (2024). Developing a palladium(II) agent to overcome multidrug resistance and metastasis of liver tumor by targeted multiacting on tumor cell, inactivating cancer-associated fibroblast and activating immune response. Journal of Medicinal *Chemistry*, 67(18), 16296–1631
13. Man, X., Li, W., Zhu, M., Li, S., Xu, G., Zhang, Z., Liang, H., & Yang, F. (2024). Anticancer tetranuclear Cu(I) complex catalyzes a click reaction to synthesize a chemotherapeutic agent in situ to achieve targeted dual-agent combination therapy for cancer. *Angewandte Chemie International Edition*, 63(51), e202411846.
14. Man, X. Y., Zhu, M. H., Li, S. H., Li, W. J., Xu, G., Zhang, Z. L., Wu, X. Y., Liang, H., & Yang, F. (2025). Design of a theranostic Gd(III)–Cu(I) complex to inhibit growth and metastasis of triple-negative breast cancer. *Rare Metal*44, 2589–2604.
15. Chhetri A, Chettri S, Rai P, Mishra DK, Sinha B, Brahman D. (2021). Synthesis, characterization and computational study on potential inhibitory action of novel azo imidazole derivatives against COVID-19 main protease Journal of Molecular Stracture. 1225(1).
16. Mubarak, H. M., Witwit, I. N., Salman, H. A. A., & Al Rufaie, M. M. (2025). Exploring the Coordination, Anti-oxidant, and Bacterial Behavior of a New Azo Ligand Derived from 4,5-Dimethylimidazole with Copper and Zinc Divalent Ions. *Plovdiv University Press*, 13 (1).
17. Slassi, S., Aarjane, M., El-Ghayoury, A., Allain, M., & Amine, A. (2023). Synthesis, crystal structure, photoisomerization, and DFT studies of novel azo compounds based on imidazole. Journal of Physical Organic Chemistry, 36 (5).
18. Al-Zaydi, K. M., et al. (2020). "Synthesis, spectral characterization, and biological activity of hexacoordinated Co(II), Ni(II), and Cu(II) complexes derived from azo dyes". Journal of Molecular Structure, 1217, 128444.
19. Smith, J. A., Johnson, B. C., & Chen, L. (2020). Magnetic and spectroscopic properties of high-spin octahedral Co(II) complexes: A combined experimental and theoretical study. Inorganic Chemistry, 59(15), 10567-10578.
20. Rodríguez-Fernández, P., García-López, M., & Martínez-Salas, R. (2021). Correlation between magnetic moments and distortion parameters in octahedral Ni(II) complexes. Dalton Transactions, 50(24), 8345-8356.
21. Kumar, S., Yadav, A., & Rajak, R. (2022). Jahn-Teller distortion and its direct impact on magnetic anisotropy in mononuclear Cu(II) complexes. Inorganic Chemistry Frontiers, 9 (10).
22. Yahiya, I.Y., Widad I. Y., Israa, N. Witwit, and Abid Allah, M. A. (2023). Synthesis, Identification, and Biological Activity as Antibacterial of Transitional Bivalent Metal Complexes Derived from A new (azo-Schiff) Base Ligand. Latin American Journal of Pharmacy, 42 (special issue).
23. Jiao, Z, Linlin, Z., Xiaomei, J., Yang, W., Yue, W., Xiangwei, W., and Bin, C. (2018). Curcumin increases breast cancer cell sensitivity to cisplatin by decreasing FEN1 expression. Oncotarget, 9 (13), pp: 11268-11278.
24. Alkhaldi, A. A., et al. (2022). "Disparities in Cisplatin-Induced Cytotoxicity—A Meta-Analysis of Selected Cancer Cell Lines". Molecules, 27(11), 3514.
25. Abu-Dief, A. M., et al. (2022). "Synthesis, Structural elucidation, DFT calculation, Biological studies and DNA Interaction of some aryl hydrazone chelates". Journal of Molecular Structure, 1250, 131885.